C. R. Physique 16 (2015) 10–25

Contents lists available at ScienceDirect

Comptes Rendus Physique

www.sciencedirect.com

Granular physics / Physique des milieux granulaires

Jamming in granular materials

Le blocage des matériaux granulaires

Robert P. Behringer

Department of Physics & Center for Non-linear and Complex Systems, Duke University, Durham, NC, USA

ARTICLE INFO

Article history:
Available online 20 February 2015

Keywords:
Granular materials
Jamming
Shear jamming
Impact
Force networks

Mots-clés :
Matériaux granulaires
Blocage
Blocage au cisaillement
Impact
Chaînes de force

ABSTRACT

Granular materials are one of a class of materials which undergo a transition from mechanically unstable to mechanically stable states as key system parameters change. Pioneering work by Liu and Nagel and O'Hern et al. focused on models consisting of frictionless grains. In this case, density, commonly expressed in terms of the packing fraction, ϕ, is of particular importance. For instance, O'Hern et al. found that there is a minimum $\phi = \phi_J$, such that below this value there are no jammed states, and that above this value, all stress-isotropic states are jammed. Recently, simulations and experiments have explored the case of grains with friction. This case is more subtle, and ϕ does not play such a simple role. Recently, several experiments have shown that there exists a range of relatively low ϕ's such that at the same ϕ it is possible to have jammed, unjammed, and fragile states in the sense of Cates et al. This review discusses some of this recent work, and contrasts the cases of jamming for frictionless and frictional granular systems.

RÉSUMÉ

Les matériaux granulaires appartiennent à une classe de matériaux qui subissent une transition d'instabilité mécanique à stabilité tandis que les paramètres du système changent. Les travaux novateurs de Liu et Nagel et O'Hern et al. ont considéré des grains sans frottement. Dans ce cas, la densité, qui est caractérisée comme d'habitude par la fraction volumique des solides ϕ, revêt une importance particulière. Par exemple, O'Hern et al. ont trouvé qu'il existe un minimum $\phi = \phi_J$ tel que, en dessous de cette valeur, il n'existe pas de blocage et que, au-dessus, tous les états où la contrainte est isotropique sont bloqués. Recemment, des simulations et des expériences ont exploré le cas de grains frottants, qui est à la fois plus subtil et où ϕ n'a plus un rôle aussi simple. Dernièrement, plusieurs expériences ont montré qu'il existe un domaine de petites valeurs de ϕ où coexistent des états bloqués, libres ou fragiles au sens de Cates et al. Cette revue aborde une partie de ces récents travaux, et compare les cas de blocage pour les systèmes granulaires frottants ou non.

E-mail address: bob@phy.duke.edu.

http://dx.doi.org/10.1016/j.crhy.2015.02.001
1631-0705/

1. Introduction

The concept of jamming, which characterizes how disordered particle systems transition from fluid-like to solid-like states, has attracted significant recent interest, in no small part due to the fact that a range of different systems undergo a jamming transition and/or exhibit glassy behavior. In some cases, the particles forming the system are truly macroscopic, as in the case of foams and granular materials. Smaller particles can occur in emulsions and colloids, and of course molecular glasses are truly microscopic. All these systems have certain features in common, such as spatial disorder and hindered motion when they are densely packed and "cold". Several reviews of jamming are available [1–3], as well as extensive reviews of glassy systems [4].

Until recently, it was thought that systems as diverse as colloids, foams, emulsions and granular materials could be unified into a single picture through a jamming diagram, involving thermodynamic temperature, T, packing fraction, ϕ, and shear stress, τ, as proposed by Liu and Nagel [5]. This proposal was intensively investigated, chiefly by numerical simulations [6–9] that modeled frictionless particles interacting via normal contact forces. Such systems can be realized experimentally as foams [3] or emulsions [10]. In this case, there is a lowest packing fraction, ϕ_J, which may depend on system preparation, below which states are always unjammed, and above which jammed states exist for a range of shear stresses, $0 \leq \tau < \tau_Y$, where $\tau_Y(\phi)$ is the yield stress. Much of that work has been reviewed recently [1–3].

The present review focuses on the nature of jamming in a particular class of macroscopic particle systems, granular materials. This term has been used broadly to label collections of macroscopic particles for which there is no mutual exchange of energy with a heat bath. For granular materials, dissipation during particle interactions injects heat into the surroundings, but the motion of grains is not affected in any substantive way by thermally heating them.

Everyday materials such as sand, salt, food grains, pharmaceutical powders or lumps of coal all qualify as 'granular materials'. All of these systems interact by contact forces: grains interact only when their surfaces are in contact, and the interaction forces are either normal to the plane of contact, or in the plane of contact, due to friction. Typically, the repulsive normal forces involve elastic deformation of the contacting particles and are conservative for slow strains, but not for fast strains. Some granular models only use conservative normal forces, i.e. the model particles are frictionless. The characteristics of jamming for frictionless and frictional particles differ in several respects, including relatively simple shifts of parameters at jamming. However, there are also much more significant differences in the types of near-jamming states for the case of frictional vs. frictionless particles.

Mechanical stability and response: At a naive level, the idea of jamming is simple: typically, disordered solid-like particle systems respond to applied strains by deforming, but without flowing; thus, jammed systems have non-zero compressional and shear moduli. Unjammed systems respond to shear strain by flowing, although, damping, e.g., viscosity or friction, may act to limit the flow.

A necessary condition for a system of particles to be jammed is that particles are mechanically stable, i.e. that they are in force and torque balance. If a system of particles is in a mechanically stable state, it is generally referred to as jammed. There may be a small set of particles, called rattlers, which are not subject to any forces. Rattlers can be removed without otherwise affecting the system. There also exist states which satisfy force and torque balance, but are not stable to particular small strains. These are fragile states, and they were first proposed by Cates et al. [11] in the context of sheared colloidal systems.

A key parameter which controls whether a system is jammed or not is the average number of contacts per particle, Z. One way to understand the role of Z is to count degrees of freedom associated with vector forces at contacts, and constraints associated with force and torque balance. For example, a system of N frictionless spheres in dimension d has $NZ/2$ independent forces, and dN force balance constraints. (Note that by Newton's third law, there are half as many independent forces as there are force-bearing contacts.) Thus, for such a system to be mechanically stable, there must be at least $Z = 2d$ contacts on average per particle. A system can have more contacts and be stable, but not less. The marginal or isostatic state exactly satisfies $Z_{\rm iso} = 2d$. A similar argument for 'ideal' frictional particles (i.e. large static friction coefficient, μ) yields an isostatic condition, $Z_{\rm iso} = d + 1$. In fact, numerical simulations [12,13] for $d = 2$ show that Z at jamming depends on μ, with a smooth variation of $Z_{\rm iso}$ between the frictionless case, where $Z_{\rm iso} = 4$ and the large-friction case where $Z_{\rm iso} = 3$.

Although the value of Z is crucial for determining whether a static state is jammed or not, it is conventional to consider the states of a system in terms of the packing fraction, ϕ and the shear stress, τ, perhaps in part because the latter two quantities are easily measured. If ϕ is too low, it is not possible for Z to reach the isostatic value. However, unlike Z, there is no theoretical argument which determines a critical value of ϕ for jamming. In general, ϕ_J depends on such system properties as dimension, particle shape and polydispersity.

By applying large enough shear stress, it is usually possible to cause a jammed state to flow. Typically, the limiting yield stress, $\tau = \tau_Y(\phi)$, needed to cause an otherwise jammed system to flow increases with ϕ. In a state space of ϕ and τ, low density states are unjammed, high density states are jammed. But for τ's lying above $\tau_Y(\phi)$, flow occurs in response to shear. This scenario is encapsulated in a jamming diagram by Liu and Nagel [5], and substantiated through numerical simulations of frictionless systems [6–9]. Fig. 1a shows a sketch of the zero-temperature plane of the Liu–Nagel (L–N) jamming diagram. A key feature of this jamming diagram is a lowest $\phi = \phi_J$, such that a) all static states with $\phi < \phi_J$ are unjammed and hence stress-free, b) ϕ_J is the terminus of the yield stress curve; c) the yield stress vanishes at ϕ_J.

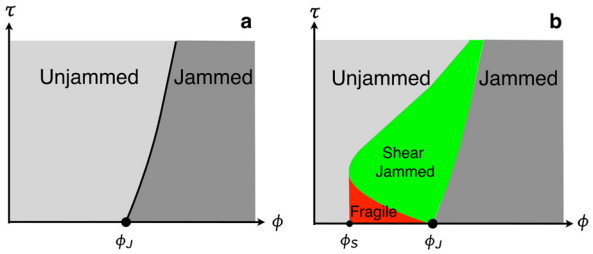

Fig. 1. Jamming diagrams in a space of shear stress, τ, and packing fraction, ϕ. These diagrams pertain to $T = 0$ systems, which include granular materials. (a) is a sketch of the Liu–Nagel diagram [5], in which states at high enough ϕ and low enough τ exist in a jammed state, the darker region. (b) is the diagram that characterizes frictional particles, as seen by Bi et al. [14]. In addition to the jammed region of the Liu–Nagel diagram, there is a region below ϕ_J, extending to a lowest density, ϕ_S, where it is possible to start from a stress-free state, apply shear strain, and arrive at a jammed state, i.e. the green region marked shear jammed. There is an intermediate region between the ϕ-axis and the shear jammed region where fragile states can exist. (For interpretation of the references to color in this figure legend, the reader is referred to the web version of this article.)

1.1. Jamming for frictionless grains

Numerical studies by O'Hern et al. [6] involved frictionless particles, and a particular protocol which involved growing the model particles, and then relaxing the system to an energy minimum. These simulations lead to several specific observations which are consistent with the L–N jamming diagram: 1) below a critical ϕ, called variously ϕ_c or ϕ_J, there are, by construction no force-bearing contacts, so $Z = 0$; 2) above ϕ_J, $Z = Z_{\rm iso} + A(\phi - \phi_J)^{\alpha}$, where $\alpha = 1/2$; 3) below ϕ_J necessarily $P = 0$; 4) above ϕ_J, the pressure increases as a power law in $\phi - \phi_J$ with an exponent, ψ that derives from the contact force law. Typically, the inter-particle force is assumed to vary with the 'overlap' at contacts: $F \propto \delta^{\psi}$. The overlap is defined in terms of the center-to-center distance $d_{i,j}$ of a pair of interacting particles: $\delta = R_i + R_j - d_{i,j}$. The repulsive normal force in these models vanishes when $d_{i,j}$ exceeds the sum of the particle radii. When $\delta > 0$ for a pair of particles, typical force models are either linear, in which case there is a repulsive force at the contact $F \propto \delta$, or Hertzian, in which case the repulsive $F \propto \delta^{3/2}$. The latter is expected for ideal spherical elastic particles.

Two other important issues for granular systems near jamming concern the response of the system to very small strains, particularly shear strain, and whether the contacts and stresses are isotropic or anisotropic. Recently, Dagois-Bohy et al. [15] have shown that certain protocols for preparing nominally isotropic jammed states of frictionless spheres can produce states near jamming, with finite pressure, that are unstable to small shear strains in certain directions. Hence, previous simulation protocols can produce states with negative shear modulus, G. These authors have developed alternative approaches to preparing jammed states that are stable to shear strain in all directions. They report states that are weakly anisotropic in terms of contacts, but that can have strongly anisotropic G, suggesting a connection to the fragile states considered by Cates et al. [11]. More recently, Goodrich et al. [16] have extensively investigated anisotropy, scaling and finite size effects, where they take care to produce states for which G does not vanish.

1.2. Jamming for frictional grains

When the particles interact by frictional as well as normal forces, the situation is more complicated. As noted, simulations show that jamming occurs at lower packing fractions as the friction coefficient, μ, grows. Several recent experiments [14,17–25] using frictional particles indicate that the jamming diagram has additional features. In Couette experiments, Howell et al. [17,26] showed that it is possible to have anisotropic states, produced by shearing collections of disks or pentagons, which have low values $\phi \simeq 0.78$ compared to $\phi_J \simeq 0.84$ for similar frictionless particles. Majmudar [19] showed that systems of disks have significantly different force networks if they have been either sheared or isotropically compressed. In a rather different direction, several authors, including Scott, Onoda and Liniger, Ojha et al. and Jerkins et al. [20,27–29] (and references therein), have investigated the existence of gravitationally stable three-dimensional packings in the low density, or random loose packing (rlp) limit. These studies have used fluidization to create loose packings as low as $\phi \simeq 0.55$ for spheres, compared to $\phi_J \simeq 0.64$, i.e. random close packing (rcp), for frictionless 3D spheres. In a different but related direction, several groups [18,23,30–32] (see also references therein) have used more local perturbations to characterize the rigidity of granular systems. For instance, Metayer et al. [23] and Geng and Behringer [18] have probed the response to shear in 3D and 2D systems, respectively, with a particular focus on changes in rigidity as a function of ϕ. In both 3D and 2D systems, there is a change in rigidity for ϕ's that are below ϕ_J for frictionless spheres.

Recently, Bi et al. [14] and Zhang et al. [22], have shown experimentally that it is possible to create a range of jammed states for ϕ's below ϕ_J for frictional spheres. Their results are shown schematically in Fig. 1b, which contains a region that is not present in the L–N diagram. These experiments have shown that for $\phi_S < \phi \leq \phi_J$, it is possible to have states at the same ϕ, which are unjammed, fragile (in the sense of Cates et al. [11]), or robustly jammed (shear jammed). The packing fraction range for this effect to occur is $\phi_S \leq \phi \leq \phi_J$, where here ϕ_J takes on a modified meaning, discussed below.

The experiments [14,22,24,25] involved applying shear strain, γ, to an initially stress-free state of 2D frictional bidisperse disks. With large enough strains, the systems reached jammed states which had $Z > 3$, positive stresses, and the ability to

resist small strains of any kind. Intermediate between the shear jammed states and the stress-free initial states were 'fragile' states in the sense of Cates et al. [11]. The resulting fragile states are anisotropic and can be unjammed easily by applying reverse strain. The lower-ϕ jammed states found in experiments have non-zero shear stress, τ. Bi et al. and Ren et al. identified ϕ_J with the largest packing fraction for which, at the same ϕ, states ranging from stress-free to shear jammed occur. Their observed value, $\phi_J \simeq 0.84$, is comparable to the jamming packing fraction determined by O'Hern et al. [6] for frictionless disks, and observed in experiments by Majmudar et al. [33]. The states generated by shear strain had anisotropic stresses and contact networks, which would be expected for systems that have been sheared. These experiments imply the jamming diagram of Fig. 1b, which below ϕ_J, contains a region of fragile states at low τ, and a region of anisotropic shear jammed states at higher τ. The two points, ϕ_J and ϕ_S in Fig. 1b have natural connections to random dense and random loose packings respectively.

Although the shear jammed states are obtained by applying shear strain to an otherwise stress-free state, shear strain is not a state variable. Rather, better descriptors [14] for characterizing states in $\phi_S < \phi < \Phi_J$ include, besides ϕ, the shear stress, the pressure, P, or the fraction of non-rattler particles, f_{NR}. Non-rattler particles have enough contacts to be mechanically stable, so at least two contacts in 2D, for frictional particles.

Before focusing specifically on jamming, it is worth noting several features of frictional granular materials in the jammed state. First, for cohesionless grains, the normal components of inter-grain contact forces point into the grain on which the force acts, and the tangential force at a contact can have a magnitude $|F_t| < \mu |F_n|$. Unlike the case of frictionless grains, a precise knowledge of the particle positions is insufficient to know the force acting at contacts, due the range of admissible tangential friction forces, for a given F_n. Second, forces are carried non-uniformly on preferred networks of connected grains called force chains [34–36], whose properties are sensitive to material properties such as friction, and also to preparation protocol (see for instance, Majmudar [19] or Kondic et al. [37] for a discussion of network topology). The structure of these networks, and degree of anisotropy are reflected in the stress and fabric tensors [19] defined below. Third, when a granular system is deformed, particularly by shear strain, these networks evolve: they grow and fail, leading to substantial spatio-temporal fluctuations of forces. Finally, shear strain leads to dilation (i.e. expansion) of a granular system if it is at least moderately densely packed, as first discovered by Reynolds [38], This effect, known as Reynolds dilatancy, implies a correlation between reductions in ϕ and increases in anisotropy due to shear. Shear jamming and Reynolds dilatancy are related phenomena, as discussed recently by Tighe [39]. Reynolds dilatancy occurs when a system is free to expand under shear strain. Shear jamming occurs when a confined system is sheared, and attains non-zero stresses.

2. Experimental approaches to understand jamming of frictional systems

The rest of this review will focus on jamming in systems of frictional particles. The original discovery of shear jamming and additional work was carried out using systems of photoelastic quasi-two-dimensional particles. The following indicates key aspects of this approach.

A typical experiment [14,17,19,22,24,33,40–54] involves applying controlled stresses or strains to systems of particles. Although the use of photoelastic particles has a long history [49–52], beginning with Howell et al. [17], experiments yielded particle-scale force information, and Majmudar and Behringer [19] first showed that it was possible to determine the vector forces at inter-particle contacts.

A basic photoelastic experiment involves placing a particle of uniform thickness, T, between crossed (typically circular) polarizers. A uniform beam of light of initial intensity I_o that traverses the particle normally will have a transmitted intensity

$$I = I_o \sin^2[(\sigma_2 - \sigma_1)\pi C T/\lambda] \tag{1}$$

where the local shear stress in the plane of the particle is $\tau = \sigma_2 - \sigma_1$. The σ_i are the principal stresses in the particle; C is the material-dependent stress optic coefficient; λ is the wavelength of the light. Note this effect is color/wavelength-dependent, and photoelastic images typically show complex colored patterns, as in Figs. 2–3, if the light source is white. The pattern within an image of a particle reflects the contact forces acting on it. Majmudar and Behringer have shown [19] that it is possible to solve a nonlinear inverse problem to obtain the individual contact forces acting on a particle, as also described elsewhere [55]. The method involves knowing the stress tensor inside the particle as a result of a set of contact forces, F_i acting on it. In the case of disks, the solution for the stress field is relatively simple, which then makes the determination of contact forces correspondingly simple. Fig. 2 shows an original color photoelastic image and the gray-scale image produced by using the fit-determined forces to reproduce the 'photoelastic' image. Since the photoelastic response is color-sensitive, only one color is used by filtering the original color image. An actual experiment involves three different types of images for each state of the system, as in the lower portion of Fig. 3. This figure shows the same small region of experiment with, left-to-right, polarizers in place, no polarizers, and with UV illumination. The first type of image yields the contact forces, the second is used for finding the centers and edges of the particles, and the last is used for determining particle rotations. Each particle has been marked with a fluorescent bar, which then enables tracking of particle rotation.

The force/contact data yield key particle-scale measures: the fabric tensor, the force moment tensor, and the stress tensor. Each of these can be coarse grained or system averaged. The fabric is a geometric measure of the contact structure:

$$R_{ij} = \frac{1}{N} \sum_{k=1}^{N} \sum_{c=1}^{c_k} n_{ik}^c n_{jk}^c \tag{2}$$

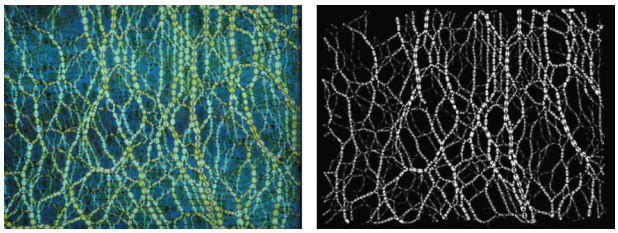

Fig. 2. (Color online.) Left: original color photoelastic image, and right: the image produced by the contact forces computed by the force-inverse algorithm for a color-filtered version of this image.

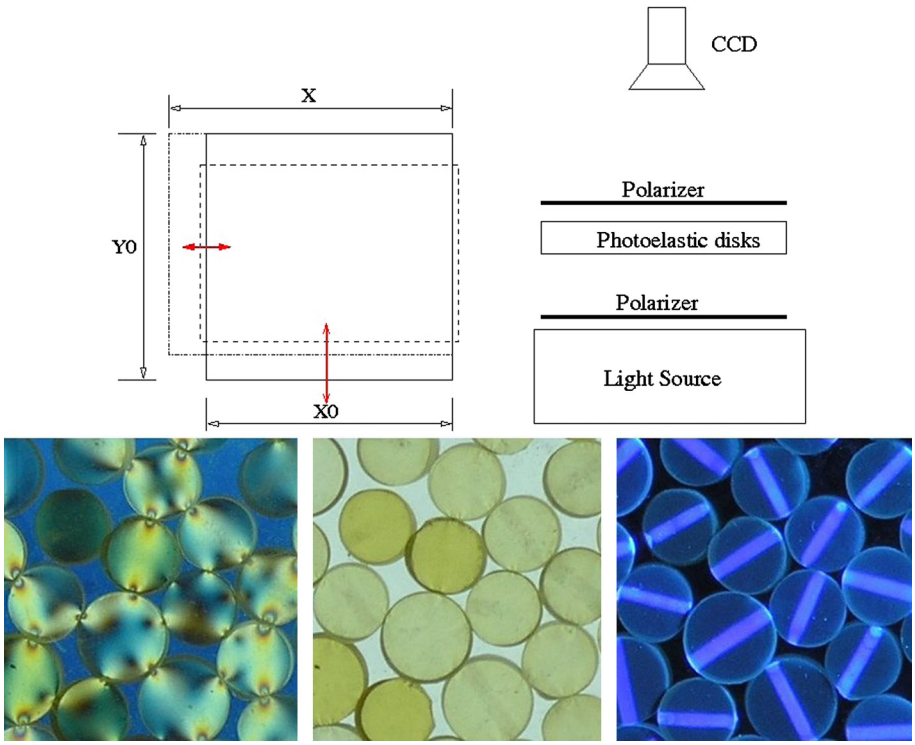

Fig. 3. (Color online.) Top: schematic of biaxial experiment; bottom: closeups showing typical experimental images. Left: photoelastic image obtained with crossed polarizers; middle: direct image without polarizers; right: imaged obtained with UV illumination, indicating the fluorescent bars used for tracking rotations.

The summation over k includes only the N non-rattler disks, c_k is the number of contacts on disk k, and n^c_{lk} is the lth component of the unit branch vector pointing from the center of the disk k to a contact c. (See Fig. 4.) A rattler disk, i.e. a disk that is not mechanically stable, and in a 2D frictional system, particles with less than two contacts are necessarily rattlers. In experiments, there is always a lower measurable force limit, which means that some contacts with non-zero force go undetected. Systems of photoelastic particles have an advantage in determining if a contact bears a force or not, since even very weak contact forces can be photoelastically detected. The average contact number, Z, is the trace of the fabric tensor R_{ij}, averaged over all particles. The difference of the eigenvalues of $\hat{R}$, $\rho = R_2 - R_1$ characterizes the anisotropy of the force network. Information on the contact network properties for some of the present experiments is given in Zhang et al. [22].

The stress and force moment tensors, σ_{ij} and, $\hat{\sigma}_{ij}$, combine information on forces and contact structure. The local force moment tensor is

$$\hat{\sigma}_{ij} = \sum_{c=1}^{c_k} f^c_{ik} r^c_{jk} \tag{3}$$

and the system-averaged stress tensor is

$$\sigma_{ij} = \frac{1}{A} \sum_{k=1}^{N} \hat{\sigma}_{ij} \tag{4}$$

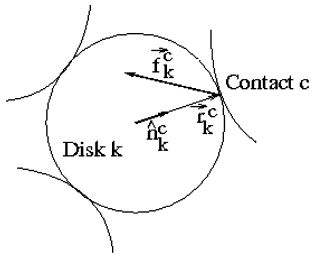

Fig. 4. Sketch explaining the notation for definitions of the fabric, force-moment and stress tensors.

(A is the system area; N, c_k, i, r^c_{jk} and j are the same as in the expression of R_{ij} and Fig. 4); here, f^c_{ik} is the ith component of the contact force on particle k at contact c. The force-moment tensor is 'extensive' since it is obtained by summing over the values for all particles. The stress tensor is a 'density'. Often, 'stress' is used to describe a coarse-grained or system-wide measure, although it is possible to also normalize the force moment tensor by the area associated to a single particle in order to produce a completely local stress measure. The eigenvalues of σ, are σ_1 and σ_2. The sum and difference of σ_1 and σ_2 divided by 2, are the pressure $P = (\sigma_2 + \sigma_1)/2$ and shear stress $\tau = (\sigma_2 - \sigma_1)/2$. By assumption in the following $\sigma_1 \leq \sigma_2$, so $\tau \geq 0$ (unless otherwise indicated).

Experiments using photoelastic particles must also involve additional apparatus which provides system-wide strains. Strains can involve Couette shear [17,26], isotropic compression [33], or shear over a limited range, which may be either pure shear [14,22] or simple shear [24,25]. The discussion below contains a brief description of the working principles for these different kinds of experiments.

3. Jamming of frictional materials

3.1. Isotropic jamming

For the photoelastic particle systems, it is possible to investigate jamming under isotropic conditions, as in Majmudar et al. [33]. In these experiments, photoelastic disks rested on a smooth Plexiglas sheet, and resided within rectangular boundaries, as sketched in Fig. 3 (top) or Fig. 5a. The experiments involved applying isotropic compression by changing the spacing between opposing pairs of boundary walls. Fig. 5d shows a typical jammed state from this type of experiment. In this case, the force chains form a dense isotropic 'tangle'. In order to try to match to the model predictions, such as those of O'Hern et al. [6], the experiment was gently 'massaged' to relax the system to a minimal stress state, following each strain increment.

Fig. 6 shows resulting experimental data for Z and P. Here, the inset, shows Z over a broad range of ϕ. The data have been analyzed to include rattlers (stars) or to exclude rattlers (squares). Note that detecting contacts is made easier due to the fact that the particles are photoelastic, as indicated by Fig. 5b.

How do these experimentally determined results compare to simulations for frictionless particles? Z grows rapidly, but not discontinuously, near $\phi_c \simeq 0.84$, as the system jams isotropically. In the simulations, below jamming there are no contacts, by definition. However, in the experiments, for the very near-jamming states, it was difficult to remove all forces, as seen in Fig. 5e. For larger ϕ, $Z(\phi)$ with/without rattlers tend to merge. $P(\phi)$ as shown in Fig. 6 has a nearly flat background value below jamming, and then grows above ϕ_c. Neither P nor Z are identically zero below jamming due to experimental noise, and more importantly, to the fact that it was very difficult to completely relax all forces/force chains for ϕ very close to but slightly less than ϕ_J. Note that these residual force chains, e.g., Fig. 5 (e), are anisotropic, which suggests that something different from isotropic jamming is coming into play.

Least squares fits of $Z - Z_c$ and P above ϕ_c to power laws in $\phi - \phi_c$ yield values of ϕ_c, β, and ψ that are consistent with the frictionless 2D model results. We obtain, $0.494 \leq \beta \leq 0.564$ excluding rattlers, and $0.363 \leq \beta \leq 0.525$ when rattlers are included. Additional details are contained in Majmudar et al. [33]. The optimum choice for ϕ_c is $\phi_c = 0.84220$. The values of β for the experimental data without rattlers is slightly larger than the value of 0.5 reported in [6–8], but smaller than the result of Donev et al. [9], who found 0.6 in 3D. Least squares fits of $P - P_c$ above ϕ_c to $P - P_c \propto (\phi - \phi_c)^{\psi}$, Fig. 6, yields $\psi = 1.1 \pm 0.05$, where, P_c corresponds to the background P. This value of ψ is consistent with the measured inter-particle interaction force, and the expected exponent based on the simulations (frictionless particles) of Silbert and O'Hern et al. [6–8].

Thus, the experiments described so far are generally consistent with the predictions for systems of frictionless grains on many, but not all, fronts. Agreement here is interesting, but not necessarily completely expected, due the differences between frictional and frictionless particles. In fact, the remnant force chains in Fig. 5 suggest that anisotropy plays a role near the jamming transition.

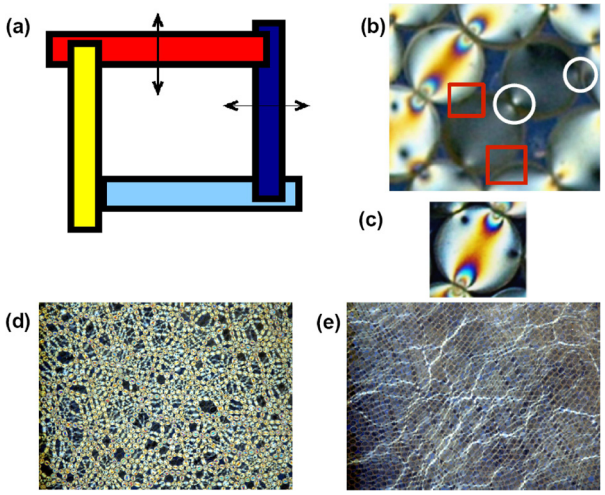

Fig. 5. (Color online.) (a) Schematic indicating the working principles of the biaxial experiments of Majmudar et al. and Bi et al. [14,19,33]. (b–c) Close-ups showing how photoelastic response helps determine where particles have a force-bearing contact. (d) Typical photoelastic image of an isotropically jammed state. (e) Photoelastic image showing weak residual force chains.

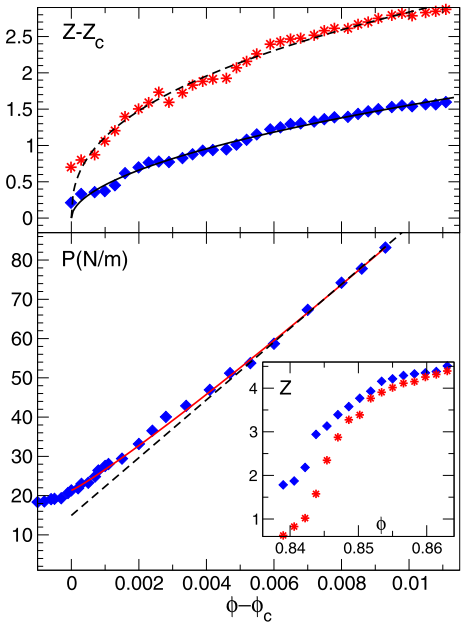

Fig. 6. (Color online.) Data for the average contact number and pressure at the jamming transition. Top $Z - Z_c$ and bottom P vs. $\phi - \phi_c$. Symbols indicate: rattlers included (stars) or excluded (diamonds). Dashed and full curves in the top panel are power-law fits $(\phi - \phi_c)^\beta$ with $\beta = 0.495$ and 0.561 (with and without rattlers, respectively). Lower panel: full curve gives the fit $(\phi - \phi_c)^\psi$ with $\psi = 1.1$; dashed line shows a linear law for comparison. Inset: Z vs. ϕ over a larger range in ϕ.

3.2. *Jamming by shear*

Recent experiments [14,22,24,25] have explored the behavior of materials in the shear jamming range of densities, $\phi_S \leq \phi \leq \phi_J$. A key characteristic of this range is that for a given density, it is possible to have states which are stress-free, fragile or robustly jammed. In these experiments, the fragile and shear jammed states were obtained by starting from a stress-free state, and by then applying shear strain. For the present purposes, it is useful to distinguish 'pure shear' and 'simple shear' strains, as in Fig. 7. In 2D pure shear, a sample is compressed in one direction and expanded in the other, all at fixed area. In simple shear, a rectangular region is mapped into a parallelogram, also at fixed area. The two types of strain are similar, except that simple shear also involves rotation.

The experiments of Zhang et al. [22] and Bi et al. [14] used the same kind of biaxial approach for systems of photoelastic disks, as in Majmudar [19,33]. In this case, one pair of opposing walls of the experiment, e.g., Figs. 3 and 5, was moved

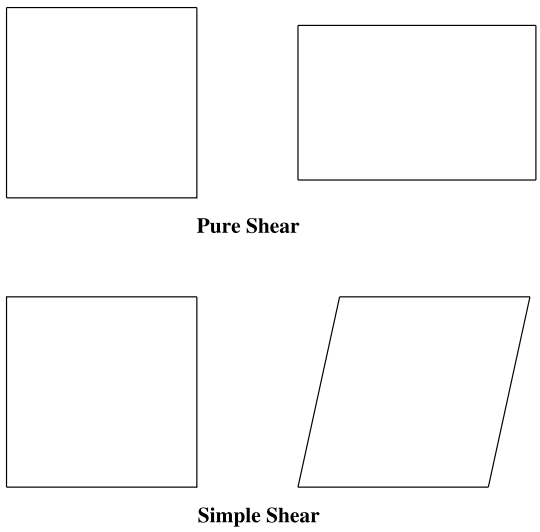

Fig. 7. Sketch contrasting pure and simple shear strains. Note that in both cases, there is one direction that expands (dilates) under shear strain, and another that is compressed. In both cases, the area occupied by the material is constant.

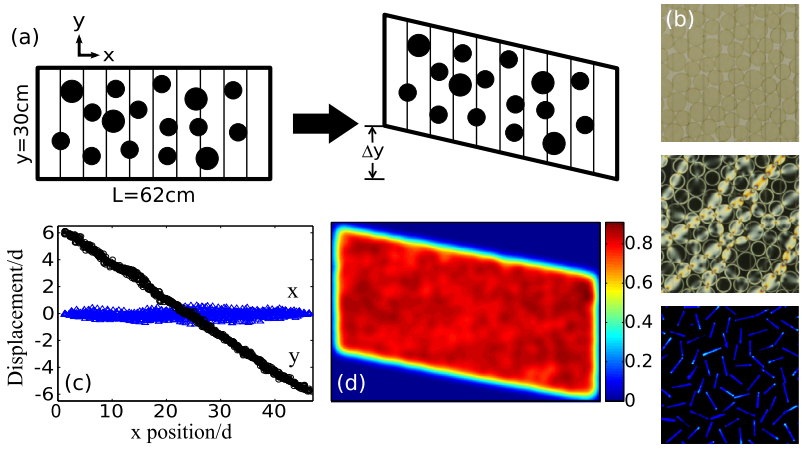

Fig. 8. (Color online.) (a) Setup schematics. (b) The three close-up images that the camera captures at each step: particle positions (upper), force response under polariscope (middle), and particle orientation images under UV light (lower). These image types are similar to those of Fig. 3 (bottom). (c) The x- and y-displacement of particles vs. their horizontal positions in the system, and (d) the coarse grained [56,57] density profile after 27% linear shear.

closer together, while the other pair was moved apart, all such that the system area remained constant. The result was pure shear strain. These experiments cleared showed the formation of fragile and strongly shear jammed states. But, during the course of shear strain, shear bands developed. As a result, there was a region of reduced density, a shear band, running diagonally across the system, with higher density regions surrounding it. This type of behavior is typical when shear is applied at the boundaries of a granular system.

In order to have a system which remains homogeneous under shear strain, Ren et al. [24] developed a new kind of experiment in which the shear strain was applied uniformly (affinely) across the sample, not just at the boundary. Fig. 8 shows a sketch of the experimental principle. The particles, photoelastic disks, rested on a set of smooth Plexiglas slats of width roughly comparable to a particle diameter. The slats moved in synchrony with the side walls to produce uniform shear strain across the system. Friction of the particles with the slats was small, but sufficient that when the system was unjammed, particles still moved in a nearly affine motion in coordination with the walls. This process provides uniform simple shear strain $\gamma = \Delta y/L$ at constant packing fraction ϕ (Fig. 8a). These experiments also used systems of photoelastic disks, (Fig. 8b) which provided detailed particle scale information, including contact forces, and particle motion. Importantly, these experiments showed no sign of a shear band or permanent inhomogeneities, e.g., Fig. 8c–d.

Although this experiment does not show failure or shear bands, as most other sheared systems do, τ, which is the difference of the principal stresses, σ_i, does reach a maximum or a plateau with increasing strain, due to the fact that the

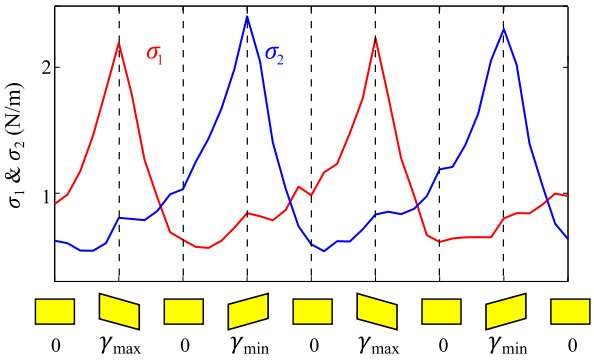

Fig. 9. (Color online.) The principal stresses for several cycles of a symmetric shear experiment. The configuration of the shear experiment is sketched underneath the data. In this case, we allow σ_1 to be greater than σ_2 by continuously tracking the eigenvalues from step to step.

system becomes more isotropic when strongly sheared. Specifically, both of the σ_i increase monotonically with γ. For large enough γ the smaller of σ_i approaches the larger. Fig. 9 shows how the σ_i vary under cyclic shearing.

Both the pure shear and simple shear experiments involved the application of small quasi-static shear strain steps. Following each step, system images yielded particle positions, photo-elastic responses, and rotations.

The application of shear strain to a stress-free state for $\phi_S \leq \phi \leq \phi_J$ leads to a series of states which are typified by the photoelastic images of Fig. 10 from Ren et al. [24]. The initial state, not shown, is free of force chains. As shear strain continues, a network for force chains first percolates from on boundary to the other in the compressive direction, as in the top figure. With continued strain, robust force chains propagate across the system in both directions, and with increasing strain, the strong force network becomes both stronger and more isotropic.

The response to shear strain involves the evolution of clusters of force chain particles, i.e. particles carrying average or above forces. A fragile state [11] occurs when the force network propagates from one boundary to the other in the compressive direction. Such a state resists continued forward shear by developing stronger force chains. But, it vanishes quickly for a small amount of shear reversal, where there are only weak contacts along the dilational direction. This is a fragile state, which is solid-like along the compressive direction, but 'squishy' along the dilational direction. By contrast, when force chains percolate in all directions, the system remains stable to small shear strain reversals. Fig. 11a shows images for the percolation of clusters across the experiment of Bi et al. [14] and the size of the clusters, as projected onto the compressive and dilational strain directions. Bi et al. [14] identify the point when the force chains percolate in the compressive direction as the onset of a fragile state, and the point where a force network first propagates in all directions as the transition to shear jamming. Fig. 11b from Bi et al. [14], summarizes the nature of many different experimental results, indicating whether they are unjammed, fragile or shear jammed.

The amount of shear strain needed to reach a shear jammed state depends on ϕ, where little shear strain is needed just below ϕ_J, and an increasingly larger γ is required as ϕ decreases towards ϕ_S, where the necessary shear strain appears to diverge. Fig. 12 shows the amount of shear strain needed to reach a shear jammed state, vs. ϕ in the experiments of Bi et al. (Here, the shear strain was represented by ϵ.) As $\phi \to \phi_S$, the amount of strain needed to obtain shear jamming grows, and eventually reaches a limit beyond with it is no longer possible to shear jam the system, at least for a given experimental apparatus.

The anisotropy in τ is necessarily correlated with anisotropy in the fabric. For instance, Fig. 13 shows the anisotropy in the fabric, defined as the difference in the principal eigenvalues of the fabric tensor, ρ, vs. τ for the data of Fig. 11.

The following argument indicates how friction facilitates this transition to shear jamming. Particles that are members of a force chain created by shear typically experience two strong, roughly diametric contacts. As a reasonable simplification, consider a force and torque balanced frictional particle, somewhere in the middle of a force chain, that experiences exactly two contacts, as sketched in Fig. 14. In a coordinate system where the x-axis bisects the angle between the two contacts, these contacts are inclined at an angle θ relative to the y-axis, as sketched. For force and torque balance, the contact forces are as sketched. The ratio of the tangential to normal components of any one of these two contact forces satisfies $F_t/F_n = \tan(\theta)$. The ratio F_t/F_n is constrained by Coulomb friction: $F_t/F_n = \tan(\theta) \leq \mu$. Thus, the smaller μ is, the more diametric the opposing contacts must be. Force chains for low friction particles must be nearly straight for pairwise contacts, whereas for higher friction particles, force chains can zigzag. In fact, force chains are buttressed by additional, often weaker, lateral contacts, which play a role in carrying force in the direction of the weaker principal stress.

As a system of frictional grains is sheared past the onset of fragility, force chains spread by developing segments in the dilational direction, thereby transmitting stress in all directions. Continued shear can distort these force chains, cause them to buckle [48], or cause individual contacts to fail. These processes can lead to added lateral contacts which make the system more homogeneous.

The anisotropy in the stress tensor, in particular, and perhaps to a lesser extent in the fabric tensor, is strongly correlated to the nearly opposing contacts that occur for grains in force chains. For the sketch of Fig. 14, a simple calculation shows

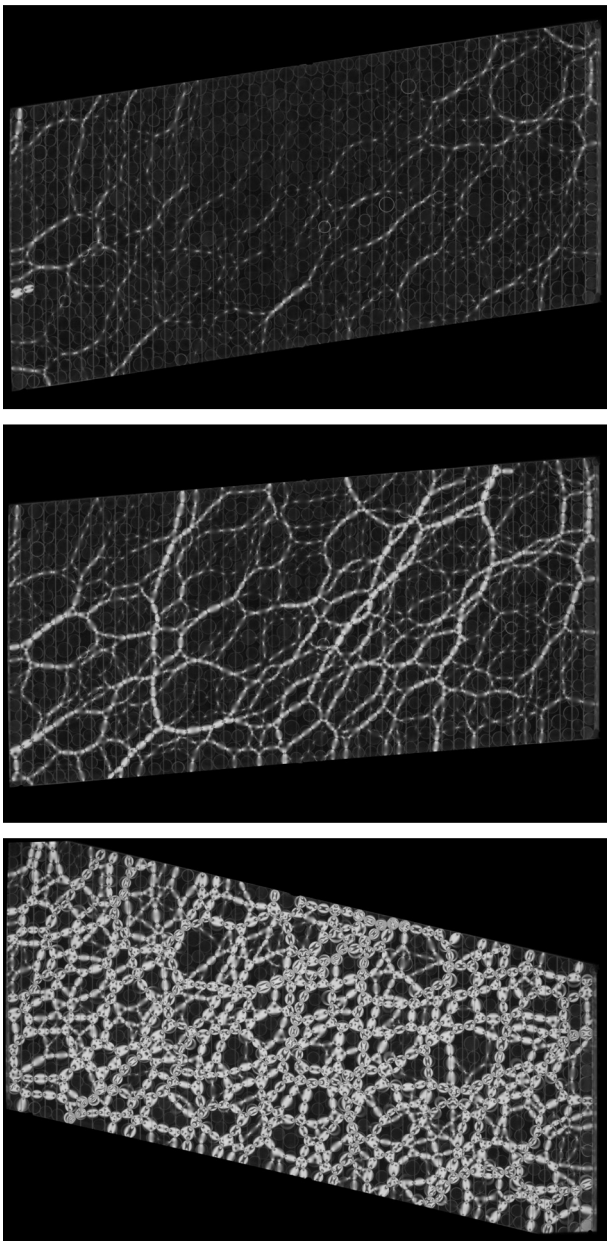

Fig. 10. Images showing the photoelastic response of disks that are subject to simple shear, after Ren et al. [24]. Top to bottom show states that are respectively fragile, near shear jamming, and well above shear jamming. In these experiments, a layer of particles is sheared, using a special apparatus that allows for uniform shear strain across the whole layer. The initial state is one that is stress free, and that has a parallelogram shape which is 'tilted down' at the lower left corner. The final state is one where the tilt is reversed. Note that throughout the shearing process, the density of the system remains constant.

that the force moment tensor for the central particle is 'maximally anisotropic' in the sense that one eigenvalue of the particle-scale force moment tensor is non-zero, and the other is zero. In this case, $P = \tau$.

The fabric tensor associated with the central particle is diagonal for this coordinate system, with components $R_{11} = 2\sin^2(\theta)$ and $R_{22} = 2\cos^2(\theta)$. Hence, the difference, $R_{22} - R_{11} = 2(\cos^2(\theta) - \sin^2(\theta) = 2\cos(2\theta)$ is nonzero, indicating local anisotropy in the fabric.

An important question is, are there state variables which can characterize the shear jammed states? Note that neither ϕ nor shear strain γ are suitable. In fact, there is a large hysteresis in P, τ and Z vs. strain, as shown in representative data for τ vs. strain (here represented by ϵ) in Fig. 15, from Zhang et al. [22]. However, a very interesting finding, shown in Fig. 16, is that a large volume of data for P and τ, which scatter broadly when expressed as a function of ϕ, collapse onto a nearly common curve when expressed as a function of f_{NR}, the fraction of non-rattler particles [14]. Likewise, data

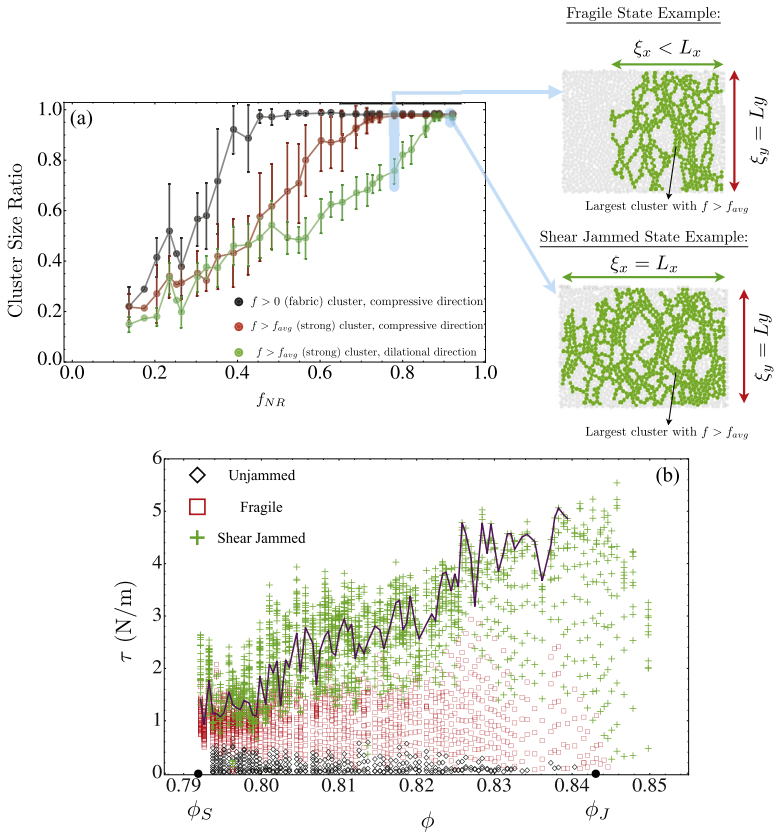

Fig. 11. (Color online.) Shear jamming properties, after Bi al. [14]. (a) contrasts fragile and shear jammed states for which a strong force network percolates in respectively, only one and both directions. Also shows cluster size normalized by the box dimension vs. f_{NR} for the fabric and strong force networks. The non-rattler fraction, f_{NR}, is discussed below. (b) gives a compilation of a large number of measurements of the shear stress, τ vs. ϕ indicating whether the state is shear jammed, fragile, unjammed and at the yield stress.

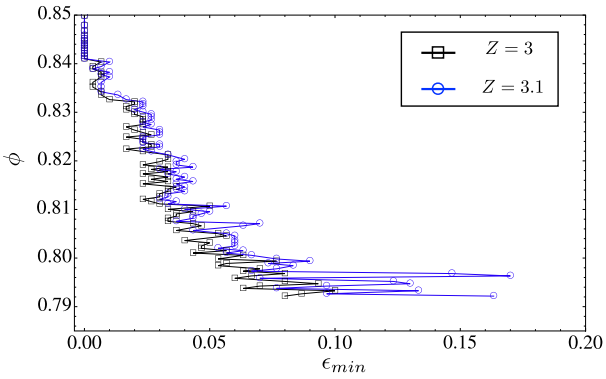

Fig. 12. (Color online.) Amount of shear strain needed for a given ϕ to reach a shear jammed state, after Bi et al. [14]. Here, shear strain is represented by the symbol ϵ.

for Z vs. f_{NR} for a broad range of ϕ in $\phi_S \leq \phi \leq \phi_J$ collapse on a common curve, as shown in Fig. 17. Note that an essential feature of suitable state variables is the representation of the system anisotropy of shear jammed states.

3.3. Nonlinear response to shear

An interesting aspect of the shear jamming regime is the growth of all components of the stress tensor from 0 as γ is increased. Since $\tau = (\sigma_2 - \sigma_1)/2$ and $P = (\sigma_2 + \sigma_1)/2$, where the signs of the σ_i can both be taken as positive, it follows that $|P| \geq |\tau|$. Thus, τ cannot increase without a corresponding increase in P. Since, P is a symmetric combination of principal stresses, it should not be sensitive to the direction of shear strain, and the experiments of Ren et al. [24] indicate that

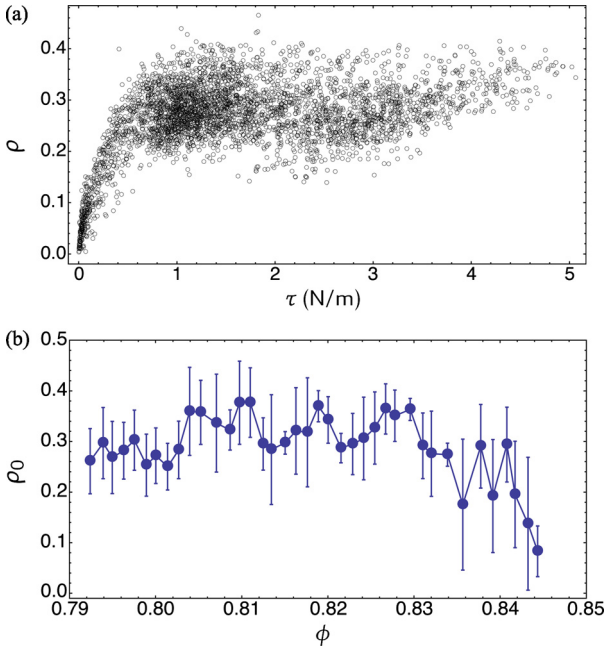

Fig. 13. (Color online.) Anisotropy in shear stress and fabric, after Bi al. [14]. (a) is a scatter plot of $\rho = R_2 - R_1$, the fabric anisotropy, vs. τ for a large collection of measurements in the shear jamming regime, $\phi_S \le \phi \le \phi_J$. (b) gives ρ at the onset of shear jamming, here identified as the point where f_{NR} reaches $f_{NR} = 0.83$.

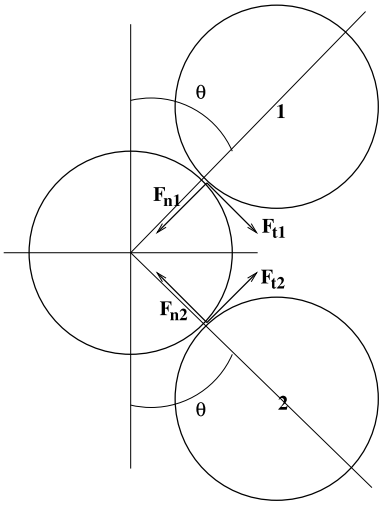

Fig. 14. Sketch of possible force and torque balanced state for a disk that has exactly two contacts with two other disks, labeled '1' and '2'. Note that the total force, i.e. the vector sum of the normal and tangential forces for each F_i, is along the y-axis.

P grows quadratically with γ as shown in Fig. 18a: P is a linear function of γ^2 to a good approximation. The 'Reynolds coefficient',

$$R = (\partial^2 P/\partial \gamma^2_{|\phi})/2 \tag{5}$$

gives a quantitative measure of the strength of the coupling between γ and P. Note that in ordinary isotropic, linear elasticity, this coupling does not exist. In this regard, a very useful discussion of the Reynolds coefficient and its relation to dilatancy and the elastic moduli is given by Tighe [39].

The Reynolds coefficient, R, is a strong function of ϕ, with an apparent divergence at $\phi = \phi_c \simeq \phi_J$. Fig. 18b and the inset, show R vs. $\Delta\phi = \phi_c - \phi$ on log–log scales. R is consistent with a power-law fit: $R = A(\phi_c - \phi)^\alpha$, with $\alpha = -3.3 \pm 0.1$ and $\phi_c = 0.841 \pm 0.004$. Hence, ϕ_c cannot be distinguished from ϕ_J. And, by comparison, ϕ_J for the present experiments (as defined by the highest ϕ for which unjammed, fragile and shear jammed states can exist) is comparable to that for systems

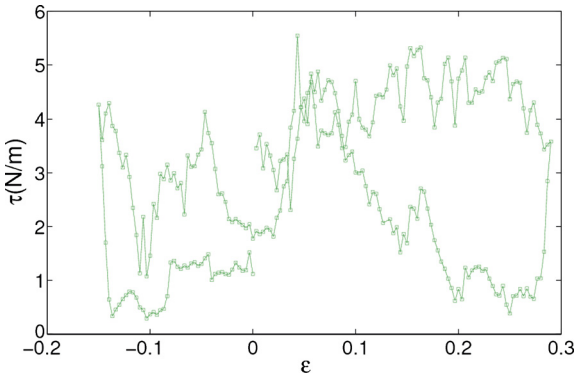

Fig. 15. (Color online.) Shear stress vs. strain for cyclic shear, showing hysteresis in τ when the sense of shear strain is reversed. (From Zhang et al. [22]; here ϵ is used for the shear strain.)

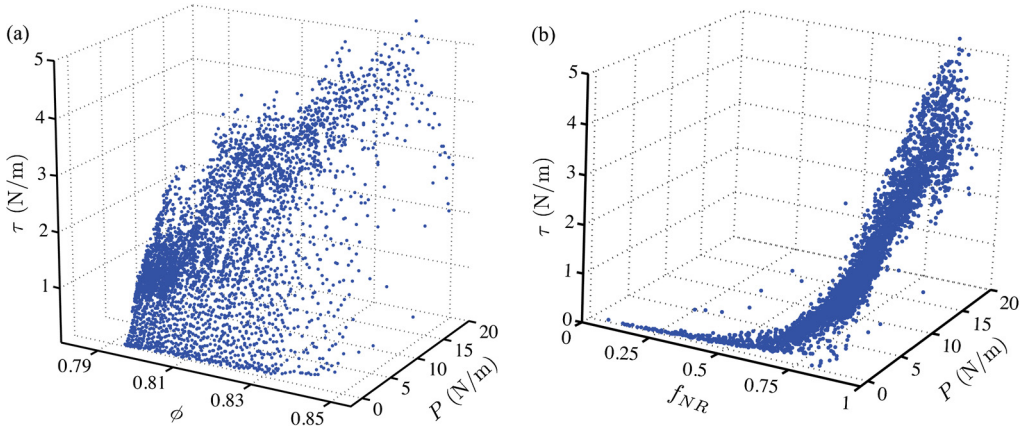

Fig. 16. (Color online.) Pressure, shear stress and the non-rattler fraction show scaling collapse. (a) P and τ as a function of ϕ for various shear experiments from Bi et al. [14]. (b) The same data plotted as a function of the non-rattler fraction, f_{NR}.

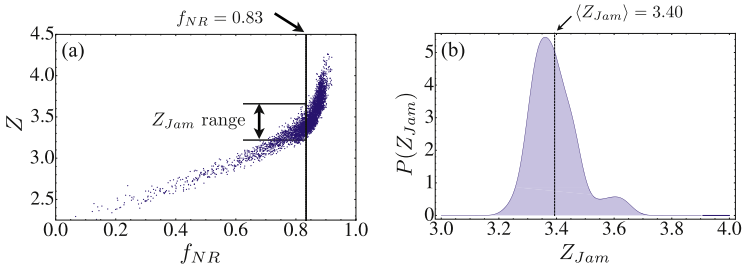

Fig. 17. (Color online.) (a) Data for Z as a function of the non-rattler fraction, f_{NR}. Note the collapse of Z when expressed as a function of f_{NR}. (b) Distribution of Z at the onset of shear jamming, taken here to be for $f_{\mathrm{NR}} = 0.83$ (from Bi et al. [14]).

of frictionless 2D particles. At the opposite extreme of density, for $\phi \leq 0.75$, percolating contact networks do not form for the largest strains available in the experiments, which are $\gamma = 54\%$.

4. Conclusions and outlook

This work has focused in particular on jamming for systems of frictional particles with circular symmetry, that is disks in 2D. Recent work has shown that the possible jammed states for this type of particle differ substantially from what is observed for models of frictionless particles. An immediate question is: are there any practical issues associated with shear jamming? Let me conclude by suggesting two settings where shear jamming occurs, and where the difference in jammed states for frictional and frictionless particles may be very significant.

Often, when a granular material is sheared, a shear band develops, as in Zhang et al. and Bi et al. [14,22]. As another concrete example, consider the Couette experiments of Howell et al. [17,26]. In these experiments, a layer of photoelastic particles (either disks or pentagons) was sheared between an inner rotating wheel of radius R (A) and a fixed outer ring (B),

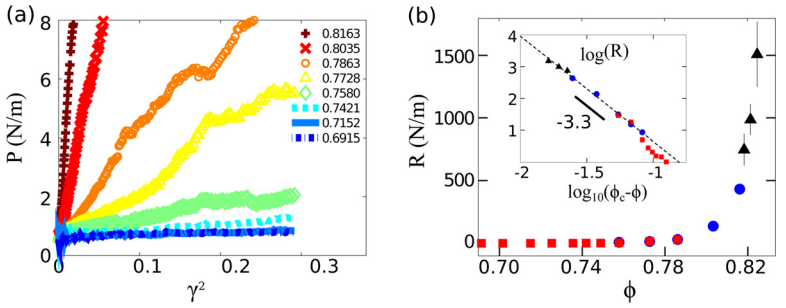

Fig. 18. (a) Reynolds pressure $P(\gamma^2)$ observed in forward shear (see text) for $\phi = 0.691 - 0.816$. (b) Reynolds coefficient R determined by appropriate least-squares fits, obtained from up to 54% forward shear (red squares), up to 27% forward shear (blue dots), and cyclic shear tests under limit cycle behavior (black triangles). The inset shows the same data on double logarithmic scales with $\phi_c = 0.841 \pm 0.004$. The error bar is smaller than the size of the symbols unless marked. The dashed line shows a fit to a power law. A line corresponding to an exponent -3.3 is also shown for reference. (For interpretation of the references to color in this figure legend, the reader is referred to the web version of this article.)

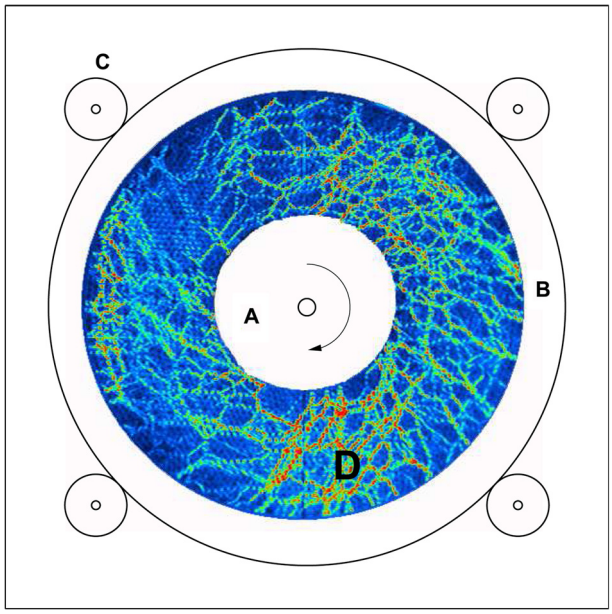

Fig. 19. (Color online.) Schematic of Couette experiment, from Howell et al. [17,26].

as in the schematic of Fig. 19. An image of the resulting force network, at one instant, is superposed on the apparatus schematic.

Fig. 20 shows the packing fraction as a function of radial distance, $(r - R)/d$ from the edge of the inner rotating wheel (here, normalized by the mean particle size, d). These data pertain to a shear jammed state. Immediately next to the shearing wheel, where $(r - R)/d \simeq 0$, the mean packing fraction is very low. Right at the wheel, ϕ is lowered due to the fact that the wheel has a much smaller curvature than any one of the particles. However, for distances from the wheel of a particle diameter or more, this geometric effect is no longer relevant. But, for distances up to about $7\,d$, the density is still low, and in fact it can be surprisingly low. This is a shear band. Note in these experiments, the strains are very slow, and the system is always very close to force balance. Force balance requires that the system is jammed over the full radial range of the experiment. The shear jammed states at low ϕ and high τ and P in the nose of the shear jamming diagram, Fig. 1b, enable the presence of the low-ϕ region associated with the shear band region, which is in force balance with a much denser region at larger distances from the shearing wheel.

A second example where shear jamming is manifested is in hopper flow. For instance, grains inside a conical shaped hopper must be unjammed to flow out of an opening at the bottom. If the opening is large, jams do not occur; if they are very small, then the hopper is blocked. For intermediate hopper openings, there may be flow which terminates when a jam occurs. Fig. 21 shows an example of a 2D hopper flow experiment [58] where a jam has occurred. Before jamming, the flow was characterized by a high degree of shear strain, and when jamming occurred, the clearly visible long force chains are indicative of static shear stresses. In this experiment, the final jammed state has a low ϕ, in the middle of the shear jamming density regime. And, the flowing state has a density that is only slightly lower on average than the final shear jammed state. Hence, at least for the experiment of Fig. 21, where it is possible to observe the details of flow and force

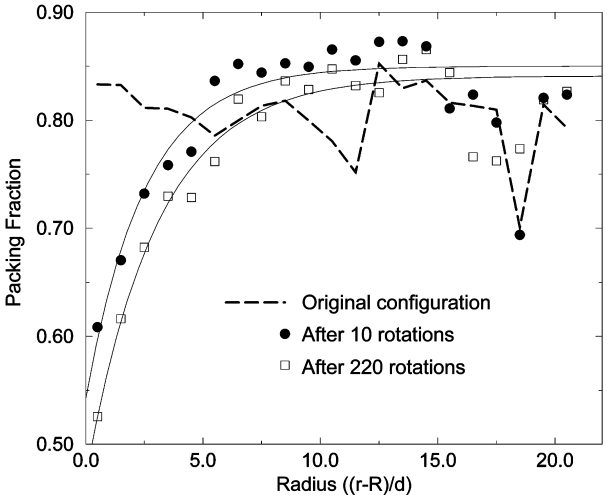

Fig. 20. Packing fraction, ϕ vs. radial distance from inner shearing wheel, showing a deep shear band (from Veje et al. [26]).

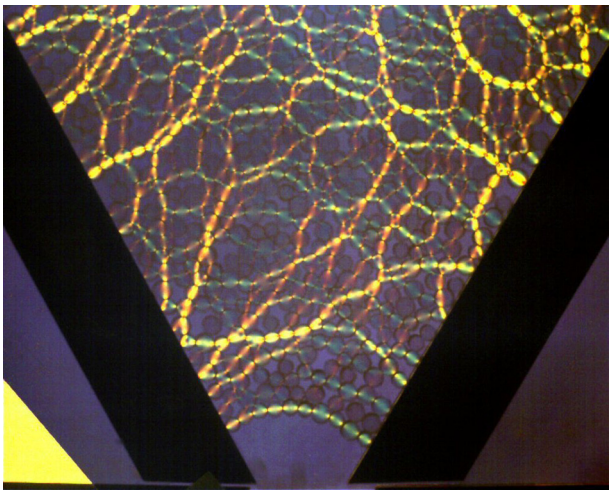

Fig. 21. (Color online.) Photoelastic image of a state from a 2D hopper experiment, after jamming (from Tang et al. [58]).

networks, the transition between flowing and jammed occurs very rapidly because the density does not have to change very much to lead to a jammed state. Thus, the possibility that unjammed, fragile and jammed states can all exist for a single density in the range $\phi_S \leq \phi \leq \phi_J$ has interesting potential consequences for granular flows. It is possible for a system to exist at one of these densities, where it is flowing, because the associated shear stress is too low for it to jam. However, it is then possible for the flowing system to jam with minimal or no density change if its shear stress increases.

In a different vein, the experiments discussed here showed that particles with friction, but that are spherical or circular have new and interesting jamming properties compared to frictionless particles. But this raises the question of how other particle properties might affect states near jamming, e.g., properties such as particle shape, perhaps coupled to friction. Of considerable interest are ways of differentiating states in the shear jamming region, since density alone is not sufficient. This has been explored in several recent studies, including Ren et al. [24] and a novel force tile representation in Sarkar et al. [59]. This is clearly an open and evolving set of issues.

Acknowledgements

This work have been supported by NSF grants DMR0906908, NSF-0835742, DMR1206351, DMS1248071, NASA grants NNX10AU01G, and NNX15AD38G, ARO grant W91NF-1-11-0110, and an IFPRI grant. Work at Duke University has been carried out by a number of collaborators, whose work is cited here. In addition, I very much appreciate constructive comments from referees, including in particular from Dr. Matthias Schröter.

References

[1] B. Chakraborty, R. Behringer, Jamming of granular matter, in: Encyclopedia of Complexity and Systems Science, vol. 39, 2009, pp. 4997–5021.
[2] M. van Hecke, J. Phys. Condens. Matter 22 (2010) 033101.
[3] Gijs Katgert, Brian P. Tighe, Martin van Hecke, Soft Matter 9 (2013) 9739.
[4] Ludovic Berthier, Giulio Biroli, Rev. Mod. Phys. 83 (2011) 587–645.
[5] A.J. Liu, S.R. Nagel, Nature 396 (1998) 21–22.
[6] C.S. O'Hern, L.E. Silbert, A.J. Liu, S.A. Langer, Phys. Rev. E 68 (2003) 011306.
[7] Leonardo E. Silbert, Gary S. Grest, James W. Landry, Phys. Rev. E 66 (2002) 061303.
[8] C.S. O'Hern, S.A. Langer, A.J. Liu, S.R. Nagel, Phys. Rev. Lett. 88 (2002) 075507.
[9] A. Donev, S. Torquato, F.H. Stillinger, Phys. Rev. E 71 (2005) 011105.
[10] J. Brujić, S.F. Edwards, D.V. Grinev, I. Hopkonson, D. Brujić, H.A. Makse, Faraday Discuss. 123 (2003) 207–220.
[11] M.E. Cates, J.P. Wittmer, J.P. Bouchaud, P. Claudin, Phys. Rev. Lett. 81 (1998) 1841.
[12] S. Henkes, M. van Hecke, W. van Saarloos, Europhys. Lett. 90 (2010) 14003.
[13] Stefanos Papanikolaou, Corey S. O'Hern, Mark D. Shattuck, Phys. Rev. Lett. 110 (2013) 1908002.
[14] D. Bi, J. Zhang, B. Chakraborty, R.P. Behringer, Nature 480 (2011) 355–358.
[15] S. Dagois-Bohy, B.P. Tighe, J. Simon, S. Henkes, M. van Hecke, Phys. Rev. Lett. 109 (2012) 095703.
[16] C.P. Goodrich, S. Dagois-Bohy, B.P. Tighe, M. van Hecke, A.J. Liu, S.R. Nagel, Phys. Rev. E 90 (2014) 022138.
[17] D. Howell, C. Veje, R.P. Behringer, Phys. Rev. Lett. 82 (1999) 5241.
[18] J. Geng, R.P. Behringer, Phys. Rev. E 71 (2005) 011302.
[19] T.S. Majmudar, R.P. Behringer, Nature 435 (2005) 1079.
[20] M. Jerkins, M. Schröter, H.L. Swinney, Phys. Rev. Lett. 101 (2008) 018301.
[21] G.E. Schröder-Turk, W. Mickel, M. Schröter, G.W. Delaney, M. Saadatfar, T.J. Senden, K. Mecke, T. Aste, Europhys. Lett. 90 (2010) 34001.
[22] J. Zhang, T.S. Majmudar, A. Tordesillas, R.P. Behringer, Granul. Matter 12 (2010) 159.
[23] J.-F. Métayer, D.J. Suntrup III, C. Radin, H.L. Swinney, M. Schröter, Europhys. Lett. 93 (2011) 64003.
[24] J. Ren, J. Dijksman, R.P. Behringer, Phys. Rev. Lett. 110 (2013) 018302.
[25] Hu Zheng, Joshua A. Dijksman, R.P. Behringer, Europhys. Lett. 107 (2014) 34006.
[26] C.T. Veje, D.W. Howell, R.P. Behringer, Phys. Rev. E 59 (1999) 739.
[27] G. Scott, Nature (London) 188 (1960) 908.
[28] G.Y. Onoda, E.G. Liniger, Phys. Rev. Lett. 64 (1990) 2727.
[29] R. Ojha, N. Moenon, D.J. Durian, Phys. Rev. E 62 (2000) 4442.
[30] I. Albert, P. Tegzes, B. Kahng, R. Albert, J.G. Sample, M. Pfeifer, A.L. Barabasi, T. Vicsek, P. Schiffer, Phys. Rev. Lett. 84 (2000) 5122.
[31] E. Kolb, J. Cviklinski, J. Lanuza, P. Claudin, E. Clement, Phys. Rev. E 69 (2004) 031306.
[32] Y. Takehara, S. Fujimoto, K. Okumura, Europhys. Lett. 92 (2010) 44003.
[33] T.S. Majmudar, M. Sperl, S. Luding, R.P. Behringer, Phys. Rev. Lett. 98 (2007) 058001.
[34] P.A. Cundall, O.D.L. Strack, Geotechnique 29 (1979) 47–65.
[35] P.A. Cundall, O.D.L. Strack, Modeling of microscopic mechanisms in granular materials, in: J.T. Jenkins, M. Satake (Eds.), Mechanics of Granular Materials: New Models and Constitutive Relations, Elsevier, Amsterdam, 1983, pp. 137–149.
[36] F. Radjai, M. Jean, J.J. Moreau, S. Roux, Phys. Rev. Lett. 77 (1996) 274.
[37] L. Kondic, A. Goullet, C.S. O'Hern, M. Kramar, K. Mischaikow, R.P. Behringer, Europhys. Lett. 97 (2012) 54001.
[38] O. Reynolds, Philos. Mag. 20 (1885) 469–481.
[39] B. Tighe, Granul. Matter 16 (2014) 201.
[40] A.P.F. Atman, P. Brunet, J. Geng, G. Reydellet, P. Claudin, R.P. Behringer, E. Clément, Eur. Phys. J. E 17 (2005) 93–100.
[41] Junfei Geng, Emily Longhi, R.P. Behringer, Phys. Rev. E 64 (2001) 060301(R).
[42] R.R. Hartley, R.P. Behringer, Nature 421 (2003) 928.
[43] J. Krim, R.P. Behringer, Phys. Today 66–67 (2009).
[44] J. Geng, D. Howell, E. Longhi, R.P. Behringer, G. Reydellet, L. Vanel, E. Clément, S. Luding, Phys. Rev. Lett. 87 (2001) 0335506.
[45] J.G. Puckett, K.E. Daniels, Phys. Rev. Lett. 110 (2013) 058001.
[46] Junfei Geng, R.P. Behringer, G. Reydellet, E. Clément, Physica D 182 (2003) 274–303.
[47] M. Da Silva, J. Rajchenbach, Nature (London) 406 (2000) 708.
[48] A. Tordesillas, J. Zhang, R.P. Behringer, Geomech. Geoengin. 4 (2009) 3–16.
[49] P. Dantu, Geotechnique 18 (1968) 50.
[50] T. Wakabayashi, J. Phys. Soc. Jpn. 5 (1950) 383–385.
[51] A. Drescher, G. De Josselin De Jong, J. Mech. Phys. Solids 20 (1972) 337.
[52] A. Drescher, Geotechnique 26 (1976) 591–601.
[53] B. Utter, R.P. Behringer, Phys. Rev. Lett. 100 (2008) 208302.
[54] D.S. Bassett, E.T. Owens, K.E. Daniels, Mason A. Porter, Phys. Rev. E 86 (2012) 041306.
[55] R.P. Behringer, Daping Bi, Bulbul Chakraborty, Abram Clark, Joshua Dijksman, Jie Ren, Jie Zhang, J. Stat. Mech. (2014) 494626.
[56] J. Zhang, R.P. Behringer, I. Goldhirsch, Prog. Theor. Phys. Suppl. 184 (2010) 16–30.
[57] A.H. Clark, P. Mort, R.P. Behringer, Granul. Matter 14 (2012), http://dx.doi.org/10.1007/s10035-011-0306-z.
[58] Junyao Tang, R.P. Behringer, Chaos 21 (2011) 041107.
[59] Sumantra Sarkar, Dapeng Bi, Jie Zhang, R.P. Behringer, Bulbul Chakraborty, Phys. Rev. Lett. 111 (2013) 068301.